JOURNAL OF COLLOID AND INTERFACE SCIENCE **178,** 144–155 (1996)
ARTICLE NO. 0102

Marangoni Retardation of the Terminal Velocity of a Settling Droplet: The Role of Surfactant Physico-Chemistry

JINNAN CHEN AND KATHLEEN J. STEBE[1]

Chemical Engineering Department, Johns Hopkins University, Baltimore, Maryland, 21218

Received April 6, 1995; accepted September 1, 1995

Nonlinear adsorption models accounting for *monolayer saturation* and *nonideal surfactant interactions* are used to find the terminal velocity U' of a droplet settling through a surfactant solution. Most prior research uses a linear adsorption model which cannot capture these effects. The solution concentration C'_{eq} is assumed to be large enough for the surfactant mass transfer to be adsorption-controlled. The Langmuir model accounts for monolayer saturation by incorporating an upper bound for the surface concentration, Γ'_∞. Two competing effects result which alter U' from that predicted by the linear model. For slow adsorption–desorption kinetics, strong Marangoni stresses develop when the surface concentration at the rear pole approaches Γ'_∞. These stresses favor *strong retardation* in U'. The adsorption flux is proportional to the unoccupied space on the interface, so depleted regions are supplied more rapidly. This diminishes Marangoni stresses and favors *weak retardation.* This effect dominates for rapid sorption kinetics. The Frumkin framework incorporates monolayer saturation and nonideal surfactant interactions which alter the amount of adsorbed surfactant, the sensitivity of the surface tension, and the dynamics of adsorptive–desorptive exchange. For a fixed mass of adsorbed surfactant, U' retarded for no interactions is increased by intersurfactant repulsion and decreased for cohesion. At elevated C'_{eq}, U' asymptotes to a value less than the Hadamard–Rybczynski velocity U'_0 for the Langmuir case and for cohesive interactions. For repulsive interactions, U' approaches U'_0 in this limit. These asymptotes indicate the degree of surface remobilization attainable for finite adsorption–desorption kinetics and nonideal interactions.

Key Words: **Marangoni stresses; surfactants; Frumkin isotherm; physico-chemical hydrodynamics, dynamic surface tension.**

1. INTRODUCTION

A droplet settling under gravity in a surfactant solution falls more slowly than a surfactant-free droplet. Surfactant adsorbs on the drop interface and reduces the surface tension. Surface convection sweeps adsorbed surfactant toward the rear of the droplet, where it accumulates, further reducing the surface tension there (see Fig. 1). The interface pulls from this low-tension region toward the leading pole, exerting a Marangoni stress which increases the drag resisting the flow, thereby retarding the terminal velocity (1). The dependence of this effect on surfactant mass transfer kinetics has been the basis of several theoretical studies. In most of these studies, *trace* surfactant adsorption is considered, and a simple linear physico-chemical framework is adopted for the adsorption isotherm and the surface equation of state. The validity of this linear framework is limited to extremely dilute concentrations.

In this work, we study the *elevated* concentration limit in which surfactant mass transfer is sorption-controlled. The role of realistic surfactant physico-chemistry in the resulting Marangoni stresses is probed using two nonlinear adsorption frameworks. The first is the Langmuir model which incorporates a maximum surface concentration, Γ'_∞, which cannot be passed for monolayer coverage. The adsorption rate is proportional to the unoccupied space on the interface. The corresponding surface equation of state gives a strong reduction in surface tension γ' when the surface concentration Γ' approaches this maximum.

The second framework studied is the Frumkin model, which accounts for surface saturation and for repulsion or cohesion between adsorbed surfactant molecules. These nonideal interactions alter the partitioning of surfactant between the bulk and the interface, the dynamics of surfactant adsorptive/desorptive exchange, and the sensitivity of the surface tension to adsorbed surfactant.

Below, the previous research in this flow field is briefly reviewed. Following this, the relevant surfactant physical chemistry and dynamics are discussed. Thereafter, the mathematical formulation and the solution technique are presented. Our results are then presented and discussed, followed by a statement of the conclusions from this study.

2. LITERATURE REVIEW

The steady surface concentration profile of adsorbed surfactant on a settling droplet is determined by the balance of surface convection along the droplet interface and exchange between the interface and the bulk fluid. If the surfactant flux from the bulk is extremely slow compared to surface convection, the surfactant behaves as an insoluble mono-

[1] To whom correspondence should be addressed.

0021-9797/96 $18.00

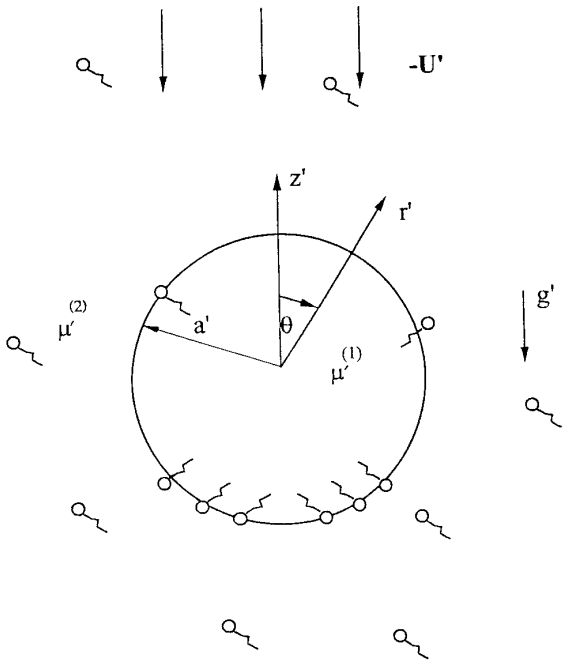

FIG. 1. The droplet is depicted in a drop-fixed reference frame. The origin of a spherical coordinate system (r', θ, ϕ) is located at the center of the droplet. The continuous phase moves with velocity U' in the $-z'$ direction under the action of gravity.

layer. In this limit, the droplet interface can be divided into two regions, the leading end, which is swept free of surfactant, and the trailing end, which is stagnated by the surfactant concentration gradient there. The size of this stagnated region is specified by a cap angle measured from the trailing pole to the edge of the stagnated region. At the opposite extreme, when the surfactant flux from the bulk is only slightly hindered compared to the surface convective flux, a surface concentration gradient develops smoothly over the entire drop surface, uniformly retarding the surface velocity continuously from leading to trailing pole. These two regimes bound the surface behavior as surfactant flux from the bulk is increased relative to the surface convection rate.

The stagnant cap regime has been investigated for small cap angles (2–4) and for arbitrary cap angles (5–8). In the arbitrary cap angle studies, the surface tension difference between the rear pole and the clean interface is related to the cap angle and terminal velocity of the droplet. In Davis and Acrivos (5) and Sadhal and Johnson (6) a linear dependence of the surface tension on the surface concentration is adopted, and the amount of adsorbed surfactant along the interface is evaluated. In He *et al.* (7) a nonlinear Langmuir adsorption framework is adopted, assuming that the extremely slow flux of surfactant from the bulk is sorption controlled. He *et al.* show that the linear equation of state underestimates the cap angle for a given Marangoni number, with the discrepancies decreasing at large Marangoni numbers.

The effect of *soluble* surfactant on the terminal and interfacial velocities of a bubble or drop has also been studied when the surfactant flux from the bulk is hindered, but not so slow as to form a stagnant cap. Levich (1) studied the uniform retardation regime, finding the reduction in the terminal velocity when the surface tension was perturbed from its equilibrium value. This limit was also examined by Wasserman and Slattery (9), who considered the effects of trace quantities of a diffusion-controlled surfactant. Levan and Newman (10) derived equations for the terminal velocity and the interfacial velocity for a droplet with an arbitrary surface tension gradient. These equations were solved for the case of an extremely dilute surfactant whose mass transport is bulk diffusion-controlled. This work was extended by Holbrook and Levan (11, 12) in a two-part study. In part one, asymptotic solutions for both the uniform retardation regime and stagnant cap regimes were derived for surfactant present in either the drop or external phase, treating both phases and all surfactant mass transfer mechanisms (adsorption–desorption, bulk diffusion, and surface diffusion) simultaneously. In part two, the intermediate retardation regime is studied where the surfactant mass transport is controlled separately by exterior diffusion, surface diffusion, or adsorption kinetics. The limiting cases of uniform retardation and stagnant cap behavior are recovered as the mass transfer mechanisms are made rapid or slow, respectively, compared to surface convection.

In most of these studies, a linear adsorption framework is adopted in which the surface tension, the surface concentration, and the bulk concentration are proportional to each other. This is valid only at extremely dilute concentrations. At higher concentrations, the linear model fails for two reasons. First, it neglects the *finite size* of surfactant molecules which precludes the surface concentration from increasing without bound. Second, the linear framework does not account for *nonideal interactions* among adsorbed surfactant molecules. In this study, surface behavior ranging from unretarded flow to near-stagnant cap behavior is studied using two nonlinear adsorption frameworks which account for these effects, viz. the Langmuir and Frumkin frameworks, which are discussed below.

3. SORPTION DYNAMICS AND THE SURFACE EQUATION OF STATE

A spherical droplet of radius a' is settling at a terminal velocity U' in an unbounded Newtonian fluid of viscosity $\mu^{(2)\prime}$. The droplet, of viscosity $\mu^{(1)\prime}$, is immiscible in the exterior phase. The outer fluid contains a surfactant at a bulk concentration C'_{eq}. (Here and throughout this article, dimensional quantities are denoted with primes, dimensionless quantities are not primed.) In the absence of motion, surfactant adsorbs along the interface, establishing an equilibrium surface concentration Γ'_{eq}. For a moving droplet, a steady, nonequilibrium surface concentration Γ' develops when the surface convective flux toward the rear of the droplet is balanced by the surfactant flux from the bulk (1):

$$\nabla_s' \cdot (\Gamma' \mathbf{V}_s') = -\mathbf{j}_r', \quad [1]$$

where $\mathbf{V}_s'$ is the surface velocity, ∇_s' is the surface gradient operator, and $-\mathbf{j}_r'$ is the flux from the bulk toward the drop surface. In this balance, surface diffusion has been neglected. In the adsorption controlled limit, diffusion instantaneously maintains a uniform bulk concentration, C_{eq}'. Using a reaction-kinetic framework (13, 14), the adsorptive flux is assumed to be first order in bulk concentration and first order in space remaining on the interface, $(\Gamma_\infty' - \Gamma')$. The desorptive flux is first order in surface concentration Γ'. The difference between these fluxes is the net flux from the bulk:

$$-\mathbf{j}_r' = \beta' C_{eq}'(\Gamma_\infty' - \Gamma') - \alpha' \Gamma'. \quad [2]$$

In this expression, β' and α' are the kinetic constants for adsorption and desorption, respectively, given by

$$\beta' = \beta_0' \exp\left(-\frac{E_a'}{R'T'}\right) \quad [3]$$

$$\alpha' = \alpha_0' \exp\left(-\frac{E_d'}{R'T'}\right). \quad [4]$$

The terms E_a' and E_d' are the energies of activation for adsorption and desorption, respectively, and $R'T'$ is the product of the ideal gas constant and the absolute temperature.

The nonuniform surface concentration Γ' establishes a nonuniform surface tension γ' which resists tangential shearing at the interface,

$$(\tau_{r\theta}^{(2)'} - \tau_{r\theta}^{(1)'})|_{r'=a'} = -\frac{1}{a'}\frac{\partial \gamma'}{\partial \theta} = -\frac{1}{a'}\frac{\partial \gamma'}{\partial \Gamma'}\frac{\partial \Gamma'}{\partial \theta}, \quad [5]$$

where $\tau_{r\theta}^{(i)'}$ is the shear stress of either the drop phase ($i = 1$) or the exterior phase ($i = 2$).

The form of $\partial\gamma'/\partial\Gamma'$ in Eq. [5] governs the coupling between the surfactant mass transfer and the stress balance. The dependence of $\gamma'(\Gamma')$ is determined by the adsorption isotherm which relates $\Gamma_{eq}'(C_{eq}')$ and by the Gibbs adsorption equation for the interface. The activation energies in Eqs. [3] and [4] must be specified to obtain the equilibrium adsorption isotherm, which is found by setting Eq. [2] to zero. For noninteracting surfactant molecules, these energies remain constant, and the Langmuir adsorption isotherm and corresponding equation of state result. However, for long chain saturated surfactants (e.g., the *n*-alcohols (13, 15)), the energies for adsorption and desorption depend upon the surface concentration because of cohesive interactions among the saturated chains. If this dependence is assumed to be linear,

$$E_i' = E_{i0}' + \nu_i' \Gamma_{eq}', \quad [6]$$

where $i = a, d$ respectively, the adsorption isotherm and surface equation of state are given by the Frumkin equations

$$\frac{\Gamma_{eq}'}{\Gamma_\infty'} = \frac{k}{e^{(-\lambda \Gamma_{eq}'/\Gamma_\infty')} + k} \quad [7]$$

$$\gamma_{eq}' = \gamma_0' + R'T'\Gamma_\infty' \times \left(\ln\left[1 - \frac{\Gamma_{eq}'}{\Gamma_\infty'}\right] + \frac{\lambda}{2}(\Gamma_{eq}'/\Gamma_\infty')^2\right), \quad [8]$$

where γ_0' and γ_{eq}' are the surface tension of the clean interface and that in equilibrium with Γ_{eq}', respectively. The adsorption number k, the ratio of the characteristic rates of adsorption to desorption, is:

$$k = \frac{\beta_0' C_{eq}'}{\alpha_0'} \exp^{-(E_{ao}' - E_{do}')/R'T'}. \quad [9]$$

In the Frumkin equations, the interaction parameter λ is introduced,

$$\lambda = \frac{(\nu_d' - \nu_a')\Gamma_\infty'}{R'T'}. \quad [10]$$

This group is positive for cohesion, negative for repulsion. For cohesion, as Γ' increases, the energy required for surfactant to desorb increases more rapidly than the activation energy for adsorption. The converse is true for repulsion. These equations reduce to the Langmuir adsorption isotherm and corresponding surface equation of state when $\nu_a' = \nu_d' = \lambda = 0$. In the equilibrium expressions (Eqs. [7] and [8]) the difference between ν_d' and ν_a' determine system behavior. However, in the surface mass balance, Eq. [1], their individual values determine surfactant adsorption and desorption kinetics. In our study, ν_a' is assumed to be zero, i.e., cohesion and repulsion are assumed to be reflected solely by changes in the desorption energy. For example, for cohesion between adsorbed surfactant, $\nu_d' > 0$, causing α' to decrease as Γ' increases, favoring more pronounced surface concentration gradients.

The nonideal interactions strongly alter the partitioning of surfactant between the bulk and the interface (13). In Fig. 2 the Frumkin isotherm, Eq. [7], is graphed. For a given C_{eq}', the $\Gamma_{eq}'/\Gamma_\infty'$ which result are greater for cohesion and smaller for repulsion when compared to the Langmuir case.

The manner in which the interactions alter $\gamma_{eq}'(\Gamma_{eq}')$ is evident from Eq. [8]. The surface tension becomes less (more) sensitive to Γ_{eq}' as cohesive (repulsive) interactions increase. On the droplet interface, the surface tension is assumed to be in local equilibrium with the surface concentra-

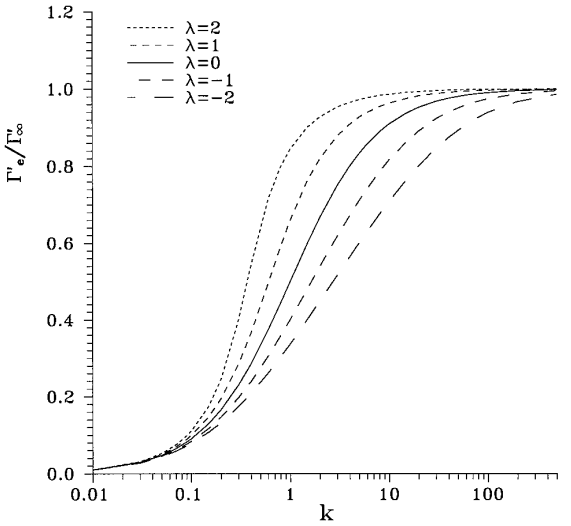

FIG. 2. The Frumkin isotherm is graphed for $\lambda = 2, 1, 0, -1, -2$. For a given k value, the $\Gamma'_{eq}/\Gamma'_{\infty}$ which result are greater for cohesion and smaller for repulsion when compared to the Langmuir case.

tion, so Eq. [8] relates $\gamma'(\Gamma')$, and the derivative of this expression determines the Marangoni stresses which must be incorporated in Eq. [5].

4. MATHEMATICAL FORMULATION

The origin of a spherical coordinate system (r', θ, ϕ) is located at the center of the droplet. In a droplet-fixed reference frame, the continuous phase moves with velocity U' in the $-z'$ direction under the action of gravity. The angle θ is measured from the front stagnation point (see Fig. 1).

In formulating the governing equations, droplet and continuous phase variables are denoted by superscripts (1) and (2), respectively. The equations are made dimensionless by scaling lengths with the droplet radius a', velocity by U', and the stress τ'_{ij} and pressure p' by $\mu^{(2)'}U'/a'$. The surface concentration is made dimensionless with Γ'_{eq}, the quantity $\Gamma'_{eq}U'/a'$ is used to scale the normal flux from the bulk, and $R'T'\Gamma'_{\infty}$ is used to scale the surface tension gradient. Since the flow is axisymmetric and incompressible, velocities may be represented by a stream function Ψ' which is nondimensionalized by a'^2U'. The steady dimensionless surface mass balance is

$$\frac{1}{\sin\theta}\frac{\partial}{\partial\theta}(\sin\theta\Gamma V_s) = \mathrm{Bi}\left[k\left(\frac{1}{y}-\Gamma\right) - \Gamma\exp(-\lambda\Gamma y)\right], \quad [11]$$

where $y = \Gamma'_{eq}/\Gamma'_{\infty}$, given by Eq. [7]. The mass balance for the Langmuir formalism is recovered by equating λ to zero in Eqs. [7] and [11].

Differentiating Eq. [8], substituting the derivative into Eq. [5], and recasting in dimensionless form, the tangential stress balance is

$$[\tau^{(2)}_{r\theta} - \kappa\tau^{(1)}_{r\theta}]|_{r=1} = \mathrm{Ma}\left[\frac{y}{1-\Gamma y} - \lambda\Gamma y^2\right]\frac{\partial\Gamma}{\partial\theta}. \quad [12]$$

Again, the Langmuir case is obtained by equating λ to zero.

In these equations, three nondimensional groups appear. These include the Biot number Bi, the ratio of characteristic desorptive flux to characteristic surface convective flux,

$$\mathrm{Bi} = \frac{\alpha_0 \exp^{-E_{a'_0}/R'T'}a'}{U'}, \quad [13]$$

the group κ, the ratio of the droplet viscosity to that of the continuous phase,

$$\kappa = \mu^{(1)'}/\mu^{(2)'}, \quad [14]$$

and, finally, the Marangoni number Ma, a ratio of characteristic Marangoni stresses to characteristic viscous stresses,

$$\mathrm{Ma} = \frac{R'T'\Gamma'_{\infty}}{\mu^{(2)'}U'}. \quad [15]$$

Stokes' equation for steady, axisymmetric, creeping flow in terms of the stream function can be written (16)

$$E^2(E^2\psi^{(i)}) = 0, \quad [16]$$

where the E^2 operator is the axisymmetric stream function operator in spherical coordinates,

$$E^2 = \frac{\partial^2}{\partial r^2} + \frac{\sin\theta}{r^2}\frac{\partial}{\partial\theta}\left(\frac{1}{\sin\theta}\frac{\partial}{\partial\theta}\right). \quad [17]$$

The velocity components can be expressed in terms of the stream function:

$$V_r^{(i)} = -\frac{1}{r^2\sin\theta}\frac{\partial\psi^{(i)}}{\partial\theta}, \quad V_\theta^{(i)} = \frac{1}{r\sin\theta}\frac{\partial\psi^{(i)}}{\partial r}. \quad [18]$$

The boundary conditions are:

(i) Far from the droplet, the uniform velocity field requires that the stream function obey

$$\lim_{r\to\infty}\psi^{(2)} = \frac{1}{2}r^2\sin^2\theta. \quad [19]$$

(ii) At the droplet center, $V_r^{(1)}$ and $V_\theta^{(1)}$ exist.

(iii) At the droplet surface, the tangential velocity components must be continuous,

$$V_\theta^{(1)}(1, \theta) = V_\theta^{(2)}(1, \theta). \quad [20]$$

(iv) The normal velocities are zero at the interface,

$$V_r^{(1)}(1, \theta) = V_r^{(2)}(1, \theta) = 0. \quad [21]$$

(v) The normal stress balance on the interface is replaced by an integral force balance which requires the integral drag force F_z' on the droplet to be balanced by the gravitational force,

$$F_z' = 2\pi\mu^{(2)'}U'a'^2 \int_0 (-p^{(2)} + \tau_{rr}^{(2)}\cos\theta - \tau_{r\theta}^{(2)}\sin\theta)\sin\theta d\theta = \frac{4}{3}\pi a'^3(\rho'^{(1)} - \rho'^{(2)})g'. \quad [22]$$

In this expression, $\rho'^{(i)}$ is the density of phase i and g' is the gravitational acceleration.

(vi) The tangential stress jump at the interface is balanced by the Marangoni stress, as expressed in Eq. [12].

5. SOLUTION TECHNIQUE

The general form of the solution of Eq. [16] in spherical coordinates can be found by separation of variables to be (16)

$$\Psi^{(i)}(r, \theta) = \sum_{n=0}^{\infty} (A_n^{(i)}r^n + B_n^{(i)}r^{-n+1} + C_n^{(i)}r^{n+2} + D_n^{(i)}r^{-n+3})C_n^{-1/2}(\cos\theta), \quad [23]$$

where $i = 1, 2$ respectively, and $C_n^{-1/2}(\cos\theta)$ is the Gegenbauer polynomial of order n and degree $-1/2$ (17).

After the boundary conditions (i) and (ii) are applied to this equation, the stream function can be rewritten in terms of the unknown coefficients $B_n^{(2)}$:

$$\Psi^{(1)}(r, \theta) = \sum_{n=2}^{\infty} B_n^{(2)}(r^n - r^{n+2})C_n^{-1/2}(\cos\theta) - \frac{U}{4}(r^2 - r^4)\sin^2\theta \quad [24]$$

$$\Psi^{(2)}(r, \theta) = \sum_{n=2}^{\infty} B_n^{(2)}(r^{-n+1} - r^{-n+3})C_n^{-1/2}(\cos\theta) + \frac{U}{2}(r^2 - r)\sin^2\theta. \quad [25]$$

The surface velocity is directly obtained from Eqs. [24], [25], and [18], and the boundary conditions (iii) and (iv) to be

$$V_s = V_\theta(1, \theta) = \frac{1}{2}\sin\theta - 2\sum_{n=2}^{\infty} B_n^{(2)}\frac{C_n^{-1/2}(\cos\theta)}{\sin\theta}. \quad [26]$$

The surfactant concentration $\Gamma(\theta)$ is expanded in Legendre polynomials,

$$\Gamma(\theta) = \sum_{m=0}^{\infty} a_m P_m(\cos\theta), \quad [27]$$

where $P_m(\cos\theta)$ is the Legendre polynomial of order m (17).

The solution entails finding the unknown coefficients $B_n^{(2)}$ and a_m. Substituting Eqs. [24] and [25] into the surface mass balance Eq. [11] and the tangential stress balance Eq. [12], two nonlinear equations result,

$$\sum_{m=0}^{\infty} a_m\Bigg[P_m(\cos\theta)\cos\theta - \frac{1}{2}m(m+1)C_{m+1}^{-1/2} \times (\cos\theta) - 2\sum_{n=2}^{\infty} B_n^{(2)}\Bigg[P_m(\cos\theta)P_{n-1}(\cos\theta) - m(m+1)\frac{C_{m+1}^{-1/2}(\cos\theta)C_n^{-1/2}(\cos\theta)}{\sin^2\theta}\Bigg] + \mathrm{Bi}kP_m(\cos\theta) + \mathrm{Bi}P_m \times (\cos\theta)e^{-\lambda y\sum_{m=0}^{\infty}a_mP_m(\cos\theta)}\Bigg] - \mathrm{Bi}k/y = 0 \quad [28]$$

and

$$\sum_{m=0}^{\infty} a_m\Bigg[1.5\kappa y\sin\theta P_m(\cos\theta) + \mathrm{Ma}ym(m+1) \times \frac{C_{m+1}^{-1/2}(\cos\theta)}{\sin\theta} - \Bigg(\mathrm{Ma}\lambda y^2 P_m(\cos\theta) \times \sum_{m=0}^{\infty} a_m m(m+1)\frac{C_{m+1}^{-1/2}(\cos\theta)}{\sin\theta}\Bigg) - y(1+\kappa)\sum_{n=2}^{\infty}(4n-2)P_m(\cos\theta)B_n^{(2)} \times \frac{C_n^{-1/2}(\cos\theta)}{\sin\theta} + \mathrm{Ma}\lambda y^3 P_m(\cos\theta) \times \sum_{m=0}^{\infty} a_m P_m(\cos\theta)\sum_{m=0}^{\infty} a_m m(m+1)$$

$$\times \frac{C_{m+1}^{-1/2}(\cos\theta)}{\sin\theta}\Bigg] + (1+\kappa)\sum_{n=2}^{\infty}(4n-2) \times B_n^{(2)}\frac{C_n^{-1/2}(\cos\theta)}{\sin\theta} - \frac{3}{2}\kappa\sin\theta = 0. \quad [29]$$

The governing equations for the Langmuir case are obtained from Eqs. [28] and [29] by setting $\lambda = 0$.

These two equations are solved simultaneously using a multiple collocation technique (18). The infinite series are truncated so as to include terms up to a_M and $B_N^{(2)}$, a total of $M + N$ unknowns. This requires $M + N$ equations which are obtained by evaluating Eqs. [28] and [29] at a total of $(M + N)/2$ equidistant, discrete collocation points along the droplet surface. The result is a set of $M + N$ nonlinear algebraic equations in terms of $M + N$ constants,

$$\sum_{m=0}^{M} a_m\Bigg[P_m(\cos\theta_i)\cos\theta_i - \frac{1}{2}m(m+1)C_{m+1}^{-1/2} \times(\cos\theta_i) - 2\sum_{n=2}^{N}B_n^{(2)} \times[P_m(\cos\theta_i)P_{n-1}(\cos\theta_i) - m(m+1) \times\frac{C_{m+1}^{-1/2}(\cos\theta_i)\,C_n^{-1/2}(\cos\theta_i)}{\sin^2\theta_i}\Bigg] + \mathrm{Bi}kP_m(\cos\theta_i) + \mathrm{Bi}P_m \times(\cos\theta_i)e^{-\lambda y\sum_{m=0}^{M}a_mP_m(\cos\theta_i)}\Bigg] - \mathrm{Bi}k/y = 0 \quad [30]$$

and

$$\sum_{m=0}^{M} a_m\Bigg[1.5\kappa y\sin\theta_i P_m(\cos\theta_i) + \mathrm{Ma}ym(m+1) \times\frac{C_{m+1}^{-1/2}(\cos\theta_i)}{\sin\theta_i} - \Bigg(\mathrm{Ma}\lambda y^2P_m(\cos\theta_i) \times\sum_{m=0}^{M}a_mm(m+1)\frac{C_{m+1}^{-1/2}(\cos\theta_i)}{\sin\theta_i}\Bigg) - y(1+\kappa)\sum_{n=2}^{N}(4n-2)P_m(\cos\theta_i)B_n^{(2)} \times\frac{C_n^{-1/2}(\cos\theta_i)}{\sin\theta_i} + \mathrm{Ma}\lambda y^3P_m(\cos\theta_i) \times\sum_{m=0}^{M}a_mP_m(\cos\theta_i)\sum_{m=0}^{M}a_mm(m+1)$$

$$\times \frac{C_{m+1}^{-1/2}(\cos\theta_i)}{\sin\theta_i}\Bigg] + (1+\kappa)\sum_{n=2}^{N}(4n-2) \times B_n^{(2)}\frac{C_n^{-1/2}(\cos\theta_i)}{\sin\theta_i} - \frac{3}{2}\kappa\sin\theta_i = 0, \quad [31]$$

where i denotes the collocation point ($i = 1, 2, \cdots (N + M)/2$). The collocation points are taken along the droplet surface ($0° < \theta < 180°$). The right-hand side of these equations is set to machine zero (i.e., 10^{-8}). The equations are solved using Newton's technique to obtain the unknown constants a_m and B_n. Initial guesses for the unknowns are obtained by an incremental process. Assuming $\mathrm{Bi} \to \infty$, analytical values for a_0–a_2 and $B_2^{(2)}$–$B_4^{(2)}$ are found from a perturbation expansion. Using small deviations from these values at finite, large Bi, values for the remaining coefficients are found to satisfy Eqs. [30] and [31]. Bi is then reduced incrementally from approximately from 50 to 0.01, using the converged values of a_m and $B_n^{(2)}$ from the previous Bi as the initial guesses.

The number of collocation points was increased until two convergence criteria were obeyed. First, the translational velocity (i.e., $B_2^{(2)}$) was required to converge to within 10^{-5}:

$$\frac{B_2^{(2)(N,M)} - B_2^{(2)(N-1,M-1)}}{B_2^{(2)(N,M)}} < 10^{-5}. \quad [32]$$

Second, $\Gamma(\theta)$ and $V_s(\theta)$ converged to within 10^{-3} at each of 37 equally spaced positions (every 5°) on the droplet surface. (In all cases, to avoid evaluation problems at the poles, the collocation points at $\theta_i = 0$ and π are replaced by closely adjacent points, i.e., $\theta_i = 0$–$0.8°$ and $\pi - 0.8°$.)

This procedure works very well for all cases. The required number of collocation points, $N + M$, increases for small values of Ma, Bi, or k (<0.1). For example, at $\kappa = 0$, Ma $= 0.5$, $k = 0.5$, and Bi < 0.1, the maximum number of collocation points required is 90 to obtain convergence. For the general inviscid bubble case, when Ma, Bi, and k are larger than unity, only 16 collocation points are needed. For $\kappa > 0$, fewer points are required for any value of Bi, k, and Ma. Similarly, for large Bi, Ma, or k, fewer points are required.

The main purpose of our calculation is to examine the effect of surfactant in reducing the droplet terminal velocity, U' which is determined by the forces acting on the fluid particle. The hydrodynamic force F_z' specified in Eq. [22] may be expressed (16)

$$F_z' = -4\pi\mu^{(2)\prime}a'U'(1 + B_2^{(2)}), \quad [33]$$

where $B_2^{(2)}$ is obtained as part of the solution of the Eqs. [30] and [31].

A surfactant-free spherical droplet of identical density and

viscosity ratios settling under gravity experiences a drag force equal to

$$F_z' = -4\pi a' U_0' \mu^{(2)'} \frac{(1 + 3\kappa/2)}{(1 + \kappa)}. \qquad [34]$$

Equating the two forces and rearranging, the ratio of the terminal velocities of the surfactant-covered droplet to the clean droplet is

$$U = \frac{U'}{U_0'} = \frac{1 + 3\kappa/2}{1 + \kappa} \frac{1}{(1 + B_2^{(2)})}. \qquad [35]$$

In addition to confirming that numerical results fell to expected limits (discussed below), an additional analytical check was made on the program. The governing equations (Eqs. [30] and [31]) were integrated numerically at zero Ma; the $\Gamma(\theta)$ obtained were confirmed to agree with the exact (analytical) solution for this limit.

6. RESULTS AND DISCUSSION

6.1. Langmuir Adsorption Framework

The terminal velocity ratio U as a function of Bi is reported in Fig. 3 for two fixed values of k; $k = 20$ (top graph) and 0.5 (bottom graph). In each figure, a family of curves

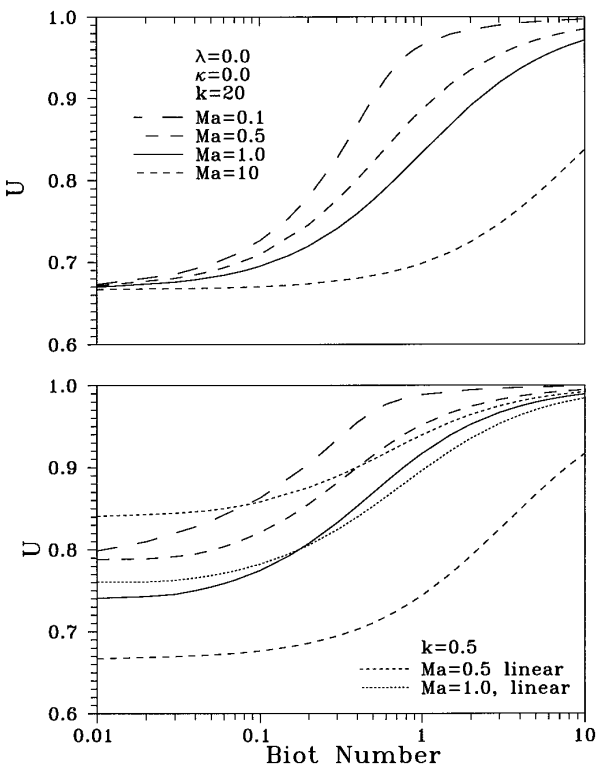

FIG. 3. The terminal velocity ratio U as a function of Bi at Ma = 0.1, 0.5, 1, 10 at $k = 20$ (top) and $k = 0.5$ with linear results for Ma = 0.5, 1 (bottom).

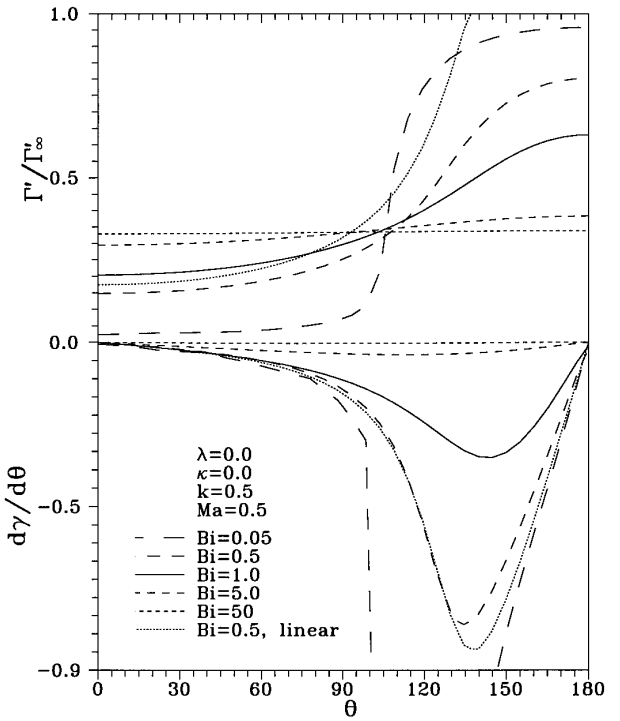

FIG. 4. The $\Gamma'(\theta)/\Gamma_\infty'$ (top) and Marangoni stress profiles (bottom) for $k = 0.5$ and Ma = 0.5 for the Langmuir framework at Bi = 0.05, 0.5, 1, 5, 50, and linear results Bi = 0.5.

is presented for various Ma. The profiles for the $k = 0.5$ case for the surface concentration $\Gamma'(\theta)/\Gamma_\infty'$ and the Marangoni stress are shown in Fig. 4. The corresponding surface velocity $V_s(\theta)$ profile is reported in Fig. 5.

For $k \ll 1$, the Langmuir framework reduces to the linear adsorption framework studied in Holbrook and Levan (12). In the linear limit, the surface equation of state is simply

$$\gamma' - \gamma_0' = R'T'\Gamma' \qquad [36]$$

with a corresponding tangential stress balance

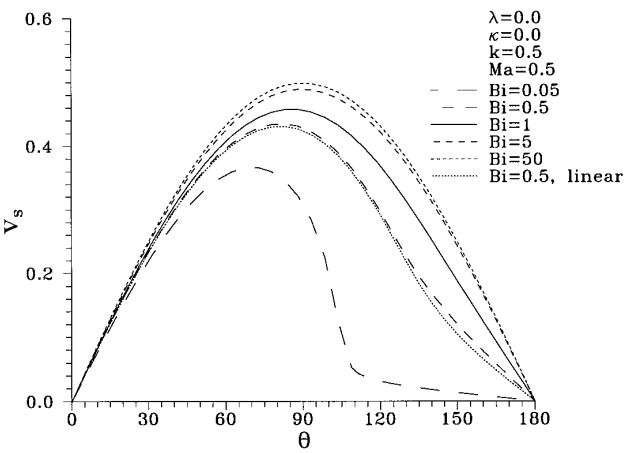

FIG. 5. The surface velocity $V_s(\theta)$ for $k = 0.5$ and Ma = 0.5 for the Langmuir framework at Bi = 0.05, 0.5, 1, 5, 50, and linear results Bi = 0.5.

$$\tau_{r\theta}^{(2)} - \kappa\tau_{r\theta}^{(1)}|_{r=1} = \mathrm{Ma}k\frac{\partial\Gamma}{\partial\theta}. \qquad [37]$$

For $k = 0.5$, the Langmuir and linear frameworks are compared at two Ma values. Departures from the linear limit are already apparent at this k value, with the linear framework underestimating the retardation for Bi less than about 0.1, and overestimating the retardation at larger Bi. These results are caused by competing effects within the Langmuir model. The Langmuir model generates nonlinear Marangoni stresses which diverge in the limit of Γ' approaching Γ_∞', strongly retarding U'. This effect competes with the adsorption flux, which is proportional to the local difference between Γ' and Γ_∞'. This tends to diminish Γ' gradients, favoring faster U'. If Γ' approaches close enough to Γ_∞', the Marangoni stress effect dominates, and stresses in excess of the linear model are generated. This is the case for extremely small Bi (see for example the results for Bi = 0.05, where Γ' at the rear pole is $0.98\Gamma_\infty'$). At higher Bi, (see, for example, the Bi = 0.5 results in Fig. 4) Γ' is never near enough to Γ_∞' to generate large Marangoni stresses, and the adsorption flux effect dominates. Surface concentration gradient for the Langmuir model are far smaller than the linear framework (which goes off the scale in Fig. 4), and the linear framework predicts a greater retardation in U'.

For both k values, U approaches unity as Bi increases. This is the expected limit; as surfactant is supplied rapidly to the interface, the surface concentration and surface tension profiles approach their uniform, equilibrium values. For example, Γ'/Γ_∞' approaches 1/3, which corresponds to $\Gamma_{\mathrm{eq}}'/\Gamma_\infty'$ for $k = 0.5$). In this limit of rapid surfactant exchange, all Marangoni stresses are eliminated, and $V_s(\theta)$ approaches its unretarded profile.

As Bi decreases, surfactant supply to the interface becomes hindered, causing greater Marangoni stresses to develop and decreasing U. As Bi tends to zero, U approaches 2/3, the Stokes velocity for all fixed values of k. This limit is approached at Bi = 0.1 for $k = 20$ in Fig. 3.

For Bi less than unity, gradients in Γ become strongly pronounced. For example, at Bi = 0.05, Γ'/Γ_∞' is less than 0.2 for $0° < \theta < 90°$, increasing rapidly to attain Γ'/Γ_∞' of 0.98 at the drop rear, near the maximum packing limit. The interface is approaching stagnant cap behavior. The surface velocity profile $V_s(\theta)$ confirms this; V_s is large at the leading end and nearly zero at the trailing end. The angle in our near-stagnant cap is estimated to be ~80° from the location of the abrupt increase in Γ'/Γ_∞' and in the Marangoni stress. This can be compared to the exact stagnant cap angle of 81° from the results of Sadhal and Johnson (6) for a droplet with the same normalized surface tension difference $((\gamma_{\max}' - \gamma_{\min}')/(\mu^{(2)\prime}U') = 1.57)$. Similar agreement is found with the results of He *et al.* (7) for their Langmuir results for $k = 0.5$ and $\mathrm{Ma}_{He} = \mathrm{Ma}U$ of 0.4.

A family of U vs k curves are presented for various Bi in Fig. 6. For all curves reported, U decreases monotonically

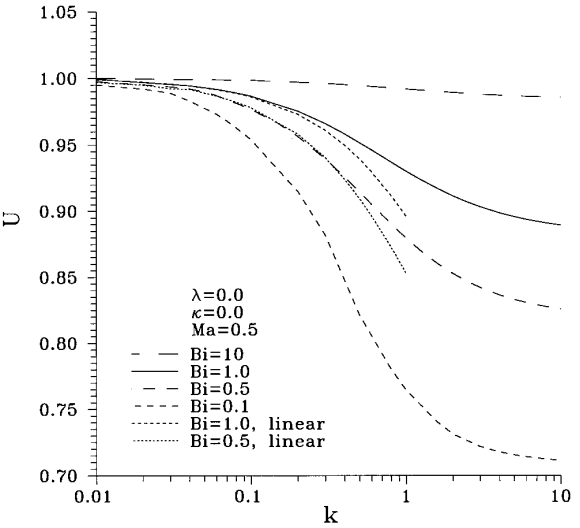

FIG. 6. The terminal velocity ratio U vs k and Ma = 0.5 for the Langmuir framework at Bi = 0.05, 0.5, 1, 5, 50 and linear results Bi = 0.5.

with k, reaching an asymptote at elevated k which increases with Bi. This result has important implications in surface remobilization, a paradigm for restoring interfacial free motion at elevated surfactant concentrations (19, 20). The essential arguments behind the surface remobilization are repeated briefly here to place this result in context.

Complete surface remobilization at elevated concentrations requires (i) rapid supply of surfactant to the droplet sublayer by bulk diffusion and (ii) rapid adsorption–desorption kinetics between the sublayer and the interface. When surface convection depletes or enriches any region on the droplet, rapid sorption and bulk diffusion restores the surface concentration to a uniform, equilibrium value. No Marangoni stresses arise, and the droplet interface behaves as a surfactant-free surface. The scaling arguments behind complete surface remobilization and the consequences of finite adsorption–desorption kinetics are outlined below.

The characteristic bulk diffusive flux of surfactant to the droplet interface is $D'C_{\mathrm{eq}}'/\delta'$ where D' is the bulk diffusivity of the surfactant and δ' is a diffusion depth. In systems with elevated bulk convective to bulk diffusive fluxes, characterized by the bulk Peclet number $\mathrm{Pe} \gg 1$, this depth is given by $a'\mathrm{Pe}^{-1/2}$, where the Peclet number Pe is

$$\mathrm{Pe} = \frac{U'a'}{D'}. \qquad [38]$$

The characteristic surface convective flux along the droplet interface is $U'\Gamma_{\mathrm{eq}}'/a'$. The ratio of the bulk diffusive flux to the interface to the surface convective flux along the interface is

$$\Lambda = \frac{1}{\sqrt{\mathrm{Pe}h}}. \qquad [39]$$

Note that Λ varies inversely with the dimensionless adsorption depth h,

$$h = \frac{\Gamma'_{eq}/C'_{eq}}{a'}, \qquad [40]$$

which approaches zero at elevated C'_{eq} since Γ'_{eq} is bounded above by Γ'_∞. As h approaches zero, Λ becomes large. In this limit, diffusion is rapid compared to the surface convective flux, and the surfactant transport is adsorption–desorption controlled.

This elevated concentration limit corresponds to elevated k. As k increases, if Γ is expanded in power of $1/k$, Γ approaches 1 to leading order,

$$\Gamma = 1 + \frac{1}{k}\Gamma_{(1)}, \qquad [41]$$

and $\Gamma_{(1)}$ is

$$\Gamma_{(1)} = -\frac{1}{\mathrm{Bi}}\frac{1}{\sin\theta}\frac{\partial}{\partial\theta}(\sin\theta V_{\theta_{(0)}})|_{r=1}. \qquad [42]$$

The leading order Marangoni stress is coupled directly to $\Gamma_{(1)}$:

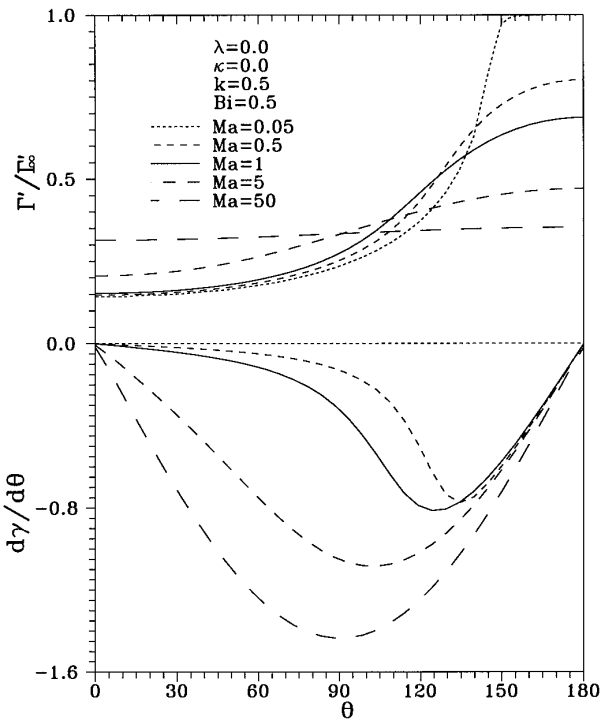

FIG. 7. The $\Gamma'(\theta)/\Gamma'_\infty$ (top) and Marangoni stress (bottom) for k = 0.5 and Bi = 0.5 for the Langmuir framework at Ma = 0.05, 0.5, 1, 5, 50.

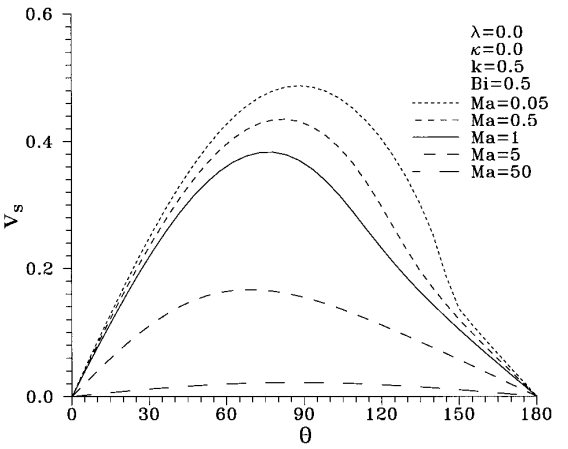

FIG. 8. The surface velocity profile $V_s(\theta)$ for k = 0.5 and Bi = 0.5 for the Langmuir framework at Ma = 0.05, 0.5, 1, 5, 50.

$$[\tau^{(2)}_{r\theta\,(0)} - \kappa\tau^{(1)}_{r\theta\,(0)}]|_{r=1} = \frac{\mathrm{Ma}}{(1-\Gamma_{(1)})}\frac{\partial\Gamma_{(1)}}{\partial\theta}. \qquad [43]$$

The Marangoni stress approaches zero, completely restoring the free motion of the interface only if the adsorption–desorption kinetics are instantaneous (Bi infinite). If, however, Bi is finite, *the elevated k limit in Fig. 6 indicates the degree of surface remobilization that can be attained.* For example, for Bi = 1, U cannot be made more rapid than 0.9 by manipulating the surfactant concentration.

The terminal velocities in Fig. 3 decrease monotonically with Ma. In Fig. 7, the profiles for Γ'/Γ'_∞ and the Marangoni stress are presented at different Ma for k fixed at 0.5. The corresponding $V_s(\theta)$ are shown in Fig. 8. As expected, as Ma increases, the retardation of the surface velocity V_s increases and the terminal velocity ratio U slows. As Ma becomes larger than unity, even small gradients in Γ can significantly retard the surface flow. For example, at Ma = 50, Γ'/Γ'_∞ deviates very slightly from its equilibrium, but V_s is strongly retarded. Conversely, the limit of small Ma relaxes the coupling between the mass transport and stress conditions. Thus the surface convective flux remains strong over the drop surface, allowing strong surface concentration gradients to develop (see Fig. 7). Even at small Ma, however, the nonlinear formalism allows sufficient stresses to develop to prevent the surface concentration from reaching the maximum packing limit. For example, consider the profiles for Ma = 0.05 of the surface concentration and the surface velocity in the vicinity of the rear pole ($\theta > 150$). The ratio Γ'/Γ'_∞ approaches 1, causing a Marangoni stress to result of sufficient strength to prevent this ratio from reaching unity. The stress is too small to be apparent in the scale of the Marangoni stress in Fig. 7, but is apparent in the shape of the surface velocity profile in Fig. 8.

All of these results were obtained at $\kappa = 0$. The droplet behavior was also studied as a function of viscosity ratio

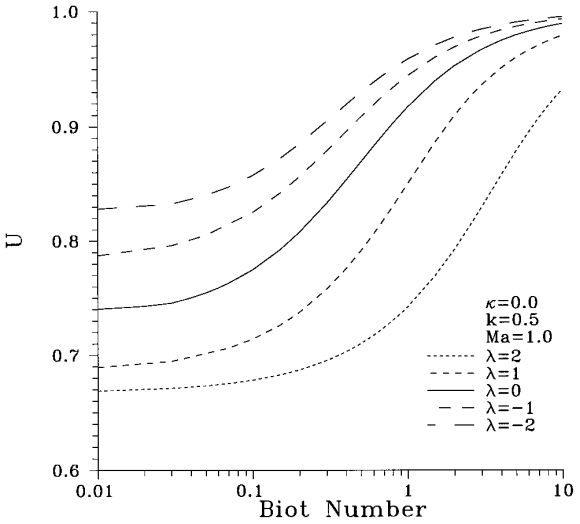

FIG. 9. The effect repulsion/cohesion on the terminal velocity U at fixed $k = 0.5$ and Ma = 1.0 at $\lambda = 2, 1, 0, -1, -2$.

κ. At small κ, the Marangoni effects were most pronounced. As κ increases, the interface became less sensitive to the Marangoni stresses. Both the surfactant-covered droplet and the surfactant-free droplet are increasingly retarded by viscous dissipation, causing both terminal velocities to approach Stokes velocity regardless of surfactant behavior. Therefore, at large κ the terminal velocity ratio U approaches 1.

6.2. Frumkin Adsorption Framework

Nonideal interactions alter surfactant behavior in dynamic systems in three ways. First, the adsorption isotherm Eq. [7] changes the partitioning of surfactant between bulk and interface (see Fig. 2), with repulsion ($\lambda < 0$) reducing the accumulation of surfactant at the interface, and cohesion ($\lambda > 0$) increasing $\Gamma'_{eq}/\Gamma'_\infty$ relative to the Langmuir case ($\lambda = 0$) at fixed k. Second, the sensitivity of the surface tension to $\Gamma'_{eq}/\Gamma'_\infty$ (Eq. [8]) increases for repulsion and decreases for cohesion relative to the Langmuir case at fixed surface coverage. Third, repulsion increases the desorption coefficient α', and cohesion decreases this kinetic constant as Γ increases (see Eq. [4]).

The effect of nonideal interactions on the terminal velocity of the droplet is shown in Fig. 9 at fixed k. Cohesion ($\lambda > 0$) reduces U, and repulsion ($\lambda < 0$) increases U at fixed bulk concentration. However, the total amount of surfactant on the interface for the different λ values differ strongly; the decrease in U might be attributed to this alone. In order to separate this effect from the surface tension dependence and desorption dynamic effects, the droplet was studied at fixed mass of adsorbed surfactant,

$$\int_0^\pi \Gamma'(\theta)/\Gamma'_\infty \sin\theta d\theta = 1.0, \qquad [44]$$

corresponding to an average surface coverage of 0.5. The results for fixed adsorbed mass for $\Gamma'(\theta)/\Gamma'_\infty$ and the Marangoni stress are presented in Fig. 10. The corresponding $V_s(\theta)$ and U vs λ are graphed in Fig. 11. These figures show that increasing λ favors stronger surface concentration gradients which generate larger Marangoni stresses. These stresses retard the surface velocity and therefore slow the terminal velocity. The effect of λ on the flow is pronounced; for strong cohesion ($\lambda = 3.5$), the interface approaches stagnant cap behavior, while for repulsion ($\lambda = -3.5$) the interface is nearly stress-free.

Cohesion reduces the sensitivity of the surface tension to surface concentration. This allows strong surface convective fluxes to force surfactant toward the drop rear pole. Since the desorption rate α' decreases as Γ' increases for cohesion, the desorption rate at the rear pole slows as surfactant accumulates there, favoring further accumulation. Thus, far larger surface concentration gradients are generated than in a Langmuir case at the same adsorbed mass, strongly retarding the surface flow. Conversely, for repulsion, areas of higher surface concentration have faster desorption kinetics, favoring a uniform surfactant distribution on the surface, and therefore generating weaker retardations.

These interactions also impact the remobilization of surfactant-laden interfaces. In Fig. 12, U is reported against k for fixed Ma and Bi. As in the Langmuir case, U asymptotes to a limiting value as k increases, indicat-

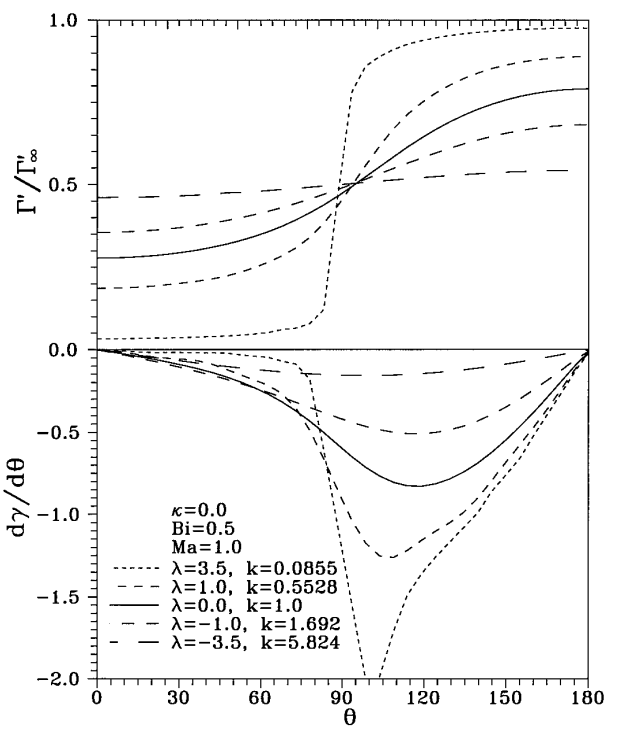

FIG. 10. The profiles for Γ'/Γ'_∞ (top) and the Marangoni stress (bottom) for $\lambda = 3.5, 1, 0, -1, -3.5$ for fixed surface mass, Bi = 0.5 and Ma = 1.0.

ing the degree of free surface motion that can be restored at elevated bulk concentrations for finite adsorption–desorption kinetics. Remobilization at elevated bulk concentration is favored by repulsion and resisted by cohesion.

7. CONCLUSIONS

The terminal velocity of a droplet settling in a surfactant solution has been studied for two nonlinear adsorption frameworks, the Langmuir model, which incorporates an upper bound to the surface concentration which can be attained in a monolayer, and the Frumkin model, which incorporates both monolayer saturation and nonideal interactions between adsorbed surfactant molecules.

The Langmuir model accounts for monolayer saturation. The model differs from the linear model in two respects. The form for the Marangoni stresses is such that a strong stress is realized when Γ'/Γ'_∞ approaches unity, favoring strong retardation of the terminal velocity in this limit. The form for the adsorption flux to the interface is proportional to the space remaining on the interface, i.e., the difference between $\Gamma'-\Gamma'_\infty$. Thus, surfactant adsorbs more rapidly to regions of the interface that are locally depleted than to those that are locally enriched. This diminishes surface concentration gradients and favors a faster terminal velocity. At slow adsorption–desorption rates, Γ'/Γ'_∞ approaches unity at the rear pole. The Marangoni stress effect dominates, and the linear framework underpredicts the retardation. At faster adsorption–desorption rates, the adsorption flux effect dominates and the linear framework overpredicts the surface retardation. At fixed Ma, the droplet terminal velocity asymptotes at elevated concentration (k) to a terminal velocity less than the Hadamard–Rybczynski value at finite adsorption–desorption kinetics. This limiting behavior indicates the degree of surface remobilization that can be attained at elevated bulk concentration of surfactant for finite adsorption–desorption kinetics.

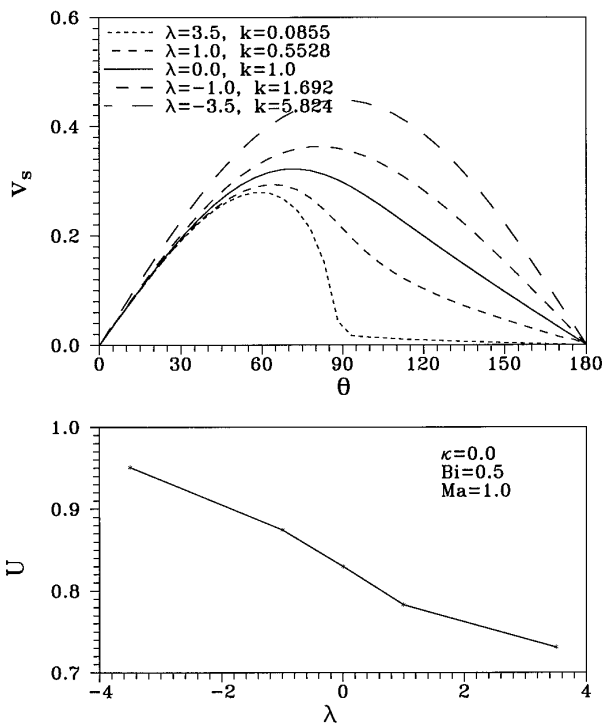

FIG. 11. The surface velocity profile $V_s(\theta)$ (top) and terminal velocity ratio U (bottom) for λ = 3.5, 1, 0, −1, −3.5 for fixed surface mass, Bi = 0.5 and Ma = 1.0.

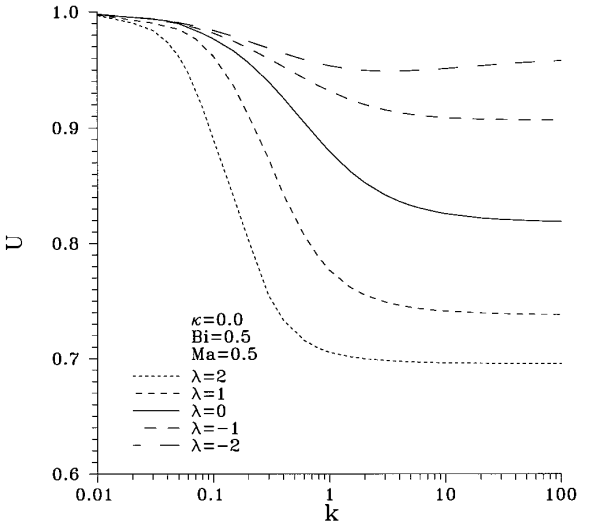

FIG. 12. The terminal velocity ratio U vs k and λ for the Frumkin model for Bi = 0.5 and Ma = 0.5.

Nonideal interactions between adsorbed surfactant also strongly alter drop behavior at fixed mass of adsorbed surfactant because of the dependence of the desorption kinetic constant α' on Γ'. For cohesive interactions, desorption slows as a function of surface concentration, leading to strong surface concentration gradients, significantly increasing droplet retardation relative to the Langmuir case. For repulsive interactions, only weak surface concentration gradients develop since desorption rates increase with surface concentration. Thus, repulsive interactions significantly reduce surface retardation relative to the Langmuir case.

As in the Langmuir case, the asymptotic values of the terminal velocity at elevated k and finite Bi indicate the degree of surface remobilization that can be realized at finite sorption kinetics. Repulsive interactions favor remobilization, while cohesive interactions disfavor it.

ACKNOWLEDGMENT

Acknowledgment is made to the Petroleum Research Fund administered by the American Chemical Society for partial support of this research.

APPENDIX: NOMENCLATURE

a_m, B_n	Expansion coefficients in Eqs. [30] and [31]
a'	Spherical bubble radius

Bi — Biot number, the ratio of characteristic desorptive flux to characteristic surface convective flux, defined in Eq. [13]
C'_{eq} — Uniform bulk concentration
$C_n^{-1/2}$ — Gegenbauer polynomial of order n and degree $-1/2$ in Eq. [23]
D' — Diffusivity of surfactant in the bulk fluid
E'_a, E'_d — The energies of activation for adsorption and desorption
F_z — Drag force, given in Eq. [22]
g' — Gravitational acceleration constant
h — Dimensionless adsorption depth, defined in Eq. [40]
$\mathbf{j}'_r$ — Molar flux of surfactant to the interface
k — Adsorption number, the ratio of the characteristic rates of adsorption to desorption, defined in Eq. [9]
Ma — Marangoni number, the ratio of characteristic Marangoni stresses to characteristic viscous stresses, defined in Eq. [15]
Pe — Peclet number, the ratio of characteristic convective to bulk diffusive fluxes, defined in Eq. [38]
P_m — Legendre polynomials in Eq. [27]
R' — The ideal gas constant
r' — radial coordinate measured from the from center of droplet
T' — The absolute temperature
$\mathbf{V}'_s$ — The surface velocity in Eq. [1]
V_r, V_θ — The velocity components in r or θ direction
U'_0 — The terminal velocity of a surfactant-free droplet or bubble
U' — The terminal velocity of the droplet or bubble under consideration
U — The terminal velocity ratio, U'/U'_0
y — The ratio of $\Gamma'_{eq}/\Gamma'_\infty$, defined in Eq. [11]
α'_0 — Desorption prefactor, defined in Eq. [4]
α' — Desorption coefficient, defined in Eq. [4]
β'_0 — Adsorption prefactor, defined in Eq. [3]
β' — Adsorption coefficient, defined in Eq. [3]
Γ'_{eq} — Surfactant surface concentration in equilibrium
Γ'_∞ — Surfactant surface concentration
Γ — Dimensionless surfactant surface concentration
γ'_0, γ'_{eq} — Surface tension of the clean interface or surface tension in equilibrium with Γ'_{eq}, respectively
κ — The viscosity ratio of droplet to continuous phase
$\mu'^{(i)}$ — Viscosity of phase i
ν'_a — Adsorption energy coefficient, defined in Eq. [6]
ν'_d — Desorption energy coefficient, defined in Eq. [6]
θ — The angular coordinate measured from the front pole stagnation point, defined in Fig. [1]
ϕ — Azimuthal angle of a spherical coordinate system
$\tau^{(i)}_{r\theta}$ — Tangential shearing stress of phase i
λ — Interaction parameter, defined in Eq. [10]
Λ — The ratio of characteristic diffusive to convective fluxes, defined in Eq. [39]
$\rho'^{(i)}$ — The density of phase i
Ψ — The stream function
∇'_s — The surface gradient operator

Subscripts

a — Adsorption
d — Desorption
m,n,N,M — The summation number

Superscripts

1 — The droplet phase
2 — The exterior phase

Prime indicates dimensional quantities, dimensionless quantities are not primed.

REFERENCES

1. Levich, V. G., ''Physicochemical Hydrodynamics,'' p. 409. Prentice Hall, Englewood Cliffs, NJ, 1962.
2. Harper, J. F., *J. Fluid Mech.* **58,** 539 (1973).
3. Harper, J. F., *Q. J. Mech. Appl. Math.* **27,** 87 (1974).
4. Harper, J. F., *Adv. Appl. Sci.* **35,** 343 (1982).
5. Davis, R. E., and Acrivos, A., *Chem. Eng. Sci.* **21,** 681 (1966).
6. Sadhal, S. S., and Johnson, R. E., *J. Fluid Mech.* **126,** 237 (1983).
7. He, Z., Maldarelli, C., and Dagan, Z., *J. Colloid Interface Sci.* **146,** 442 (1991).
8. Oguz, H. N., and Sadhal, S. S., *J. Fluid Mech.* **194,** 563 (1988).
9. Wasserman, M. L., and Slattery, J. C., *AIChE J.* **15,** 533 (1969).
10. Levan, M. D., and Newman, J., *AIChE J.* **22,** 695 (1976).
11. Holbrook, J. A., and Levan, M. D., *Chem. Eng. Commun.* **20,** 191 (1983).
12. Holbrook, J. A., and Levan, M. D., *Chem. Eng. Commun.* **20,** 273 (1983).
13. Lin, S. Y., McKeigue, K., and Maldarelli, C., *Langmuir* **10,** 3442 (1994).
14. Aveyard, R., and Haydon, D. A., ''Introduction to the Principles of Surface Chemistry.'' Cambridge Univ. Press, Cambridge, UK, 1973.
15. Fainerman, V. B., and Lylyk, S. V., *Kolloidn. Zh.* **44,** 598 (1982).
16. Happel, H., and Brenner, H., ''Low Reynolds Number Hydrodynamic.'' Noordhoof, Leyden, 1973.
17. Abramowitz, M., and Stegun, I. A. ''Handbook of Mathematical Functions.'' Dover, New York, 1970.
18. Finlayson, B. A., ''The Method of Weighted Residuals and Variational Principles.'' Academic Press, New York, 1972.
19. Stebe, K. J., Lin, S. Y., and Maldarelli, C., *Phys. Fluids A.* **3,** 3 (1991).
20. Stebe, K. J., and Maldarelli, C., *J. Colloid Interface Sci.* **163,** 177 (1994).